

# The Oceanic Sink for Anthropogenic CO<sub>2</sub>

Christopher L. Sabine,<sup>1\*</sup> Richard A. Feely,<sup>1</sup> Nicolas Gruber,<sup>2</sup>  
Robert M. Key,<sup>3</sup> Kitack Lee,<sup>4</sup> John L. Bullister,<sup>1</sup> Rik Wanninkhof,<sup>5</sup>  
C. S. Wong,<sup>6</sup> Douglas W. R. Wallace,<sup>7</sup> Bronte Tilbrook,<sup>8</sup>  
Frank J. Millero,<sup>9</sup> Tsung-Hung Peng,<sup>5</sup> Alexander Kozyr,<sup>10</sup>  
Tsueno Ono,<sup>11</sup> Aida F. Rios<sup>12</sup>

Using inorganic carbon measurements from an international survey effort in the 1990s and a tracer-based separation technique, we estimate a global oceanic anthropogenic carbon dioxide (CO<sub>2</sub>) sink for the period from 1800 to 1994 of  $118 \pm 19$  petagrams of carbon. The oceanic sink accounts for  $\sim 48\%$  of the total fossil-fuel and cement-manufacturing emissions, implying that the terrestrial biosphere was a net source of CO<sub>2</sub> to the atmosphere of about  $39 \pm 28$  petagrams of carbon for this period. The current fraction of total anthropogenic CO<sub>2</sub> emissions stored in the ocean appears to be about one-third of the long-term potential.

Since the beginning of the industrial period in the late 18th century, i.e., over the anthropocene (1), humankind has emitted large quantities of CO<sub>2</sub> into the atmosphere, mainly as a result of fossil-fuel burning, but also because of land-use practices, e.g., deforestation (2). Measurements and reconstructions of the atmospheric CO<sub>2</sub> history reveal, however, that less than half of these emissions remain in the atmosphere (3). The anthropogenic CO<sub>2</sub> that did not accumulate in the atmosphere must have been taken up by the ocean, by the land biosphere, or by a combination of both. The

relative roles of the ocean and land biosphere as sinks for anthropogenic CO<sub>2</sub> over the anthropocene are currently not known. Although the anthropogenic CO<sub>2</sub> budget for the past two decades, i.e., the 1980s and 1990s, has been investigated in detail (3), the estimates of the ocean sink have not been based on direct measurements of changes in the oceanic inventory of dissolved inorganic carbon (DIC).

Recognizing the need to constrain the oceanic uptake, transport, and storage of anthropogenic CO<sub>2</sub> for the anthropocene and to provide a baseline for future estimates of oceanic CO<sub>2</sub> uptake, two international ocean research programs, the World Ocean Circulation Experiment (WOCE) and the Joint Global Ocean Flux Study (JGOFS), jointly conducted a comprehensive survey of inorganic carbon distributions in the global ocean in the 1990s (4). After completion of the U.S. field program in 1998, a 5-year effort was begun to compile and rigorously quality-control the U.S. and international data sets, in-

cluding a few pre-WOCE data sets in regions that were data limited (5). The final data set consists of 9618 hydrographic stations collected on 95 cruises, which represents the most accurate and comprehensive view of the global ocean inorganic carbon distribution available (6). As individual basins were completed, the ocean tracer-based  $\Delta C^*$  method (7) was used to separate the anthropogenic CO<sub>2</sub> component from the measured DIC concentrations (8–10). Here we synthesize the individual ocean estimates to provide an ocean data-constrained global estimate of the cumulative oceanic sink for anthropogenic CO<sub>2</sub> for the period from  $\sim 1800$  to 1994 (11).

**Distribution and inventories of anthropogenic CO<sub>2</sub> in the ocean.** The objectively gridded individual sample estimates were vertically integrated to produce the column inventory map shown in Fig. 1. Because the global survey had limited data coverage in the marginal basins and the Arctic Ocean (north of 65°N), these areas were excluded from the mapped regions. The cumulative oceanic anthropogenic CO<sub>2</sub> sink in 1994, for the ocean region shown in Fig. 1, is  $106 \pm 17$  Pg C. Accounting for the excluded regions, we estimate a global anthropogenic CO<sub>2</sub> sink of  $118 \pm 19$  Pg C. The uncertainty in the total inventory is based on uncertainties in the anthropogenic CO<sub>2</sub> estimates and mapping errors (11).

Figure 1 shows that this anthropogenic CO<sub>2</sub> is not evenly distributed throughout the oceans. The highest vertically integrated concentrations are found in the North Atlantic. As a result, this ocean basin stores 23% of the global oceanic anthropogenic CO<sub>2</sub>, despite covering only 15% of the global ocean area (table S1). By contrast, the Southern Ocean south of 50°S has very low vertically integrated anthropogenic CO<sub>2</sub> concentrations, containing only 9% of the global inventory. More than 40% of the global inventory is found in the region between 50°S and 14°S

<sup>1</sup>National Oceanic and Atmospheric Administration (NOAA) Pacific Marine Environmental Laboratory, 7600 Sand Point Way NE, Seattle, WA 98115, USA. <sup>2</sup>University of California–Los Angeles, Institute of Geophysics and Planetary Physics and Department of Atmospheric and Oceanic Sciences, Los Angeles, CA 90095, USA. <sup>3</sup>Princeton University, Program in Atmospheric and Oceanic Science, Forrestal Campus/Sayre Hall, Princeton, NJ 08544, USA. <sup>4</sup>Pohang University of Science and Technology, San 31, Nam-gu, Hyoja-dong, Pohang 790-784, South Korea. <sup>5</sup>NOAA Atlantic Oceanographic and Meteorological Laboratory, 4301 Rickenbacker Causeway, Miami, FL 33149, USA. <sup>6</sup>Institute of Ocean Sciences, Climate Chemistry Laboratory, Post Office Box 6000, Sidney, BC V8L 4B2, Canada. <sup>7</sup>Forschungsbereich Marine Biogeochemie, Leibniz Institut für Meereswissenschaften, an der Universität Kiel, (IFM-GEOMAR), Düsternbrooker Weg 20, D-24105 Kiel, Germany. <sup>8</sup>Commonwealth Scientific and Industrial Research Organisation (CSIRO) Marine Research and Antarctic Climate and Ecosystem Cooperative Research Center, Hobart, Tasmania 7001, Australia. <sup>9</sup>University of Miami, Rosenstiel School of Marine and Atmospheric Science, Division of Marine and Atmospheric Sciences, 4600 Rickenbacker Causeway, Miami, FL 33149, USA. <sup>10</sup>Carbon Dioxide Information Analysis Center, Oak Ridge National Laboratory, U.S. Department of Energy, Mail Stop 6335, Oak Ridge, TN 37831–6335, USA. <sup>11</sup>Frontier Research System for Global Change/Institute for Global Change Research, Sumitomo Hamamatsu-cho, Building 4F, 1-18-16 Hamamatsutyo, Minato-ku, 105-0013, Japan. <sup>12</sup>Instituto de Investigaciones Marinas, Consejo Superior de Investigaciones Científicas, c/Eduardo Cabello, 6, 36208 Vigo, Spain.

\*To whom correspondence should be addressed. E-mail: chris.sabine@noaa.gov

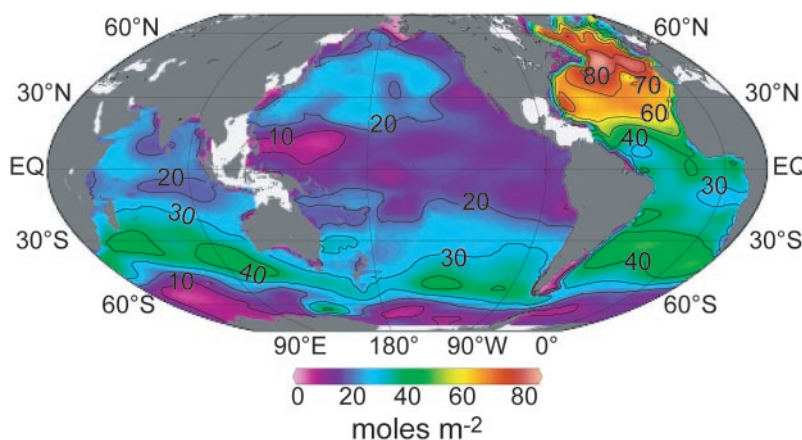


**Fig. 1.** Column inventory of anthropogenic CO<sub>2</sub> in the ocean (mol m<sup>-2</sup>). High inventories are associated with deep water formation in the North Atlantic and intermediate and mode water formation between 30° and 50°S. Total inventory of shaded regions is  $106 \pm 17$  Pg C.

because of the substantially higher vertically integrated concentrations and the large ocean area in these latitude bands (Fig. 1, table S1). About 60% of the total oceanic anthropogenic  $\text{CO}_2$  inventory is stored in the Southern Hemisphere oceans, roughly in proportion to the larger ocean area of this hemisphere.

Figure 2 shows the anthropogenic  $\text{CO}_2$  distributions along representative meridional sections in the Atlantic, Pacific, and Indian oceans for the mid-1990s. Because anthropogenic  $\text{CO}_2$  invades the ocean by gas exchange across the air-sea interface, the highest concentrations of anthropogenic  $\text{CO}_2$  are found in near-surface waters. Away from deep water formation regions, the time scales for mixing of near-surface waters downward into the deep ocean can be centuries, and as of the mid-1990s, the

anthropogenic  $\text{CO}_2$  concentration in most of the deep ocean remained below the detection limit for the  $\Delta C^*$  technique.

Variations in surface concentrations are related to the length of time that the waters have been exposed to the atmosphere and to the buffer capacity, or Revelle factor, for seawater (12, 13). This factor describes how the partial pressure of  $\text{CO}_2$  in seawater ( $P_{\text{CO}_2}$ ) changes for a given change in DIC. Its value is proportional to the ratio between DIC and alkalinity, where the latter term describes the oceanic charge balance. Low Revelle factors are generally found in the warm tropical and subtropical waters, and high Revelle factors are found in the cold high latitude waters (Fig. 3). The capacity for ocean waters to take up anthropogenic  $\text{CO}_2$  from the atmosphere is inversely proportional to the value of the Revelle factor; hence, the

lower the Revelle factor, the higher the oceanic equilibrium concentration of anthropogenic  $\text{CO}_2$  for a given atmospheric  $\text{CO}_2$  perturbation. The highest anthropogenic  $\text{CO}_2$  concentrations ( $\sim 60 \mu\text{mol kg}^{-1}$ ) are found in the subtropical Atlantic surface waters because of the low Revelle factors in that region. By contrast, the near-surface waters of the North Pacific have a higher Revelle factor at comparable latitudes and consequently lower anthropogenic  $\text{CO}_2$  concentrations primarily because North Pacific alkalinity values are as much as  $100 \mu\text{mol kg}^{-1}$  lower than those in the North Atlantic (Fig. 3).

About 30% of the anthropogenic  $\text{CO}_2$  is found at depths shallower than 200 m and nearly 50% at depths above 400 m. The global average depth of the  $5 \mu\text{mol kg}^{-1}$  contour is  $\sim 1000$  m. The majority of the anthropogenic  $\text{CO}_2$  in the ocean is, therefore, confined to the thermocline, i.e., the region of the upper ocean where temperature changes rapidly with depth. Variations in the penetration depth of anthropogenic  $\text{CO}_2$  that has accumulated in the near-surface waters is transported into the ocean interior. This transport occurs primarily along surfaces of constant density called isopycnal surfaces.

The deepest penetrations are associated with convergence zones at temperate latitudes where water that has recently been in contact with the atmosphere can be transported into the ocean interior. The isopycnal surfaces in these regions tend to be thick and inclined, providing a pathway for the movement of anthropogenic  $\text{CO}_2$ -laden waters into the ocean interior. Low vertical penetration is generally observed in regions of upwelling, such as the Equatorial Pacific, where intermediate-depth waters, low in anthropogenic  $\text{CO}_2$ , are transported toward the surface. The isopycnal layers in the tropical thermocline tend to be shallow and thin, minimizing the movement of anthropogenic  $\text{CO}_2$ -laden waters into the ocean interior.

Figure 4A shows the distribution of anthropogenic  $\text{CO}_2$  on a relatively shallow isopycnal surface (see depths in Fig. 2) with a potential density ( $\sigma_\theta$ ) of 26.0. About 20% of the anthropogenic  $\text{CO}_2$  is stored in waters with potential densities equal to or less than that of this surface. The highest concentrations are generally found closest to where this density intersects the surface, an area referred to as the outcrop. Concentrations decrease away from these outcrops in the Indian and Pacific oceans, primarily reflecting the aging of these waters, i.e., these waters were exposed to lower atmospheric  $\text{CO}_2$  concentrations when they were last in contact with the atmosphere. The Atlantic waters do not show this trend because the 26.0  $\sigma_\theta$  surface is much shallower and therefore relatively well connected to the ventilated surface waters throughout most of the Atlantic (Figs. 2A and 4A).

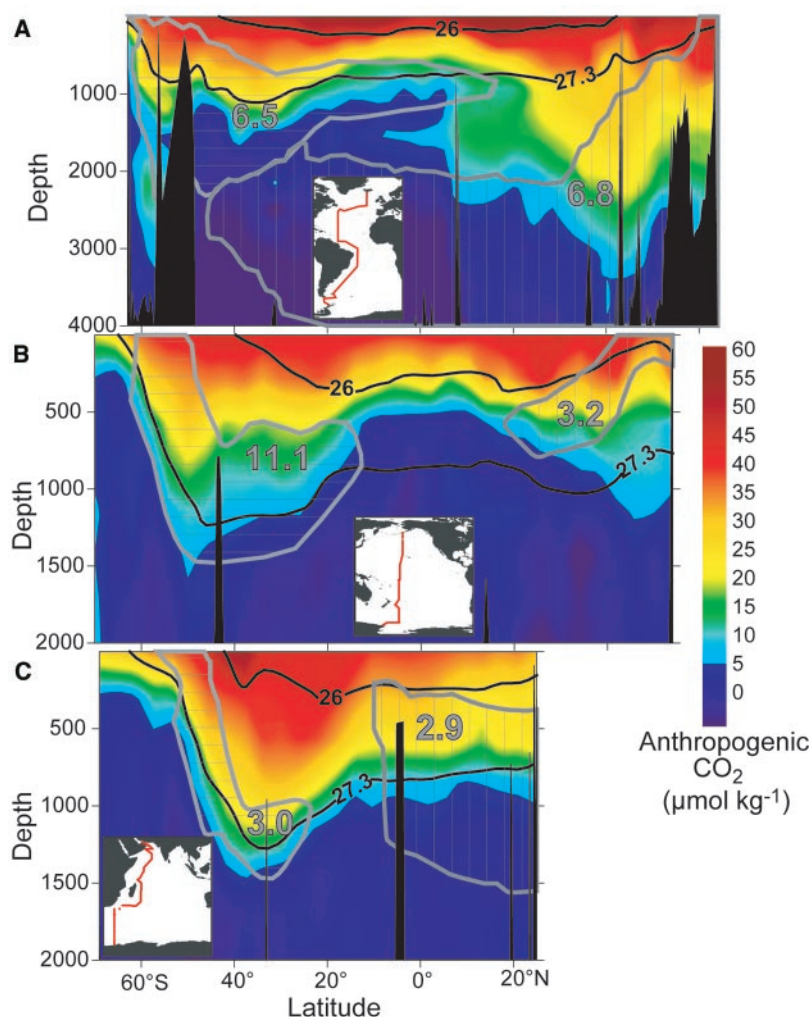


**Fig. 2.** Representative sections of anthropogenic  $\text{CO}_2$  ( $\mu\text{mol kg}^{-1}$ ) from (A) the Atlantic, (B) Pacific, and Indian (C) oceans. Gray hatched regions and numbers indicate distribution of intermediate water masses (and North Atlantic Deep Water) on the given section and the total inventory of anthropogenic  $\text{CO}_2$  (Pg C) within these water masses. The southern water masses in each ocean represent Antarctic Intermediate Water. The northern water masses represent the North Atlantic Deep Water (A), North Pacific Intermediate Water (B), and Red Sea/Persian Gulf Intermediate Water (C). The two bold lines in each panel give the potential density [ $\sigma_\theta = (\text{density} - 1) \times 1000$ ] contours for the surfaces shown in Fig. 4. Insets show maps of the cruise tracks used. Note that the depth scale for (A) is twice that of the other figures, reflecting the deeper penetration in the North Atlantic.



The formation and transport of mode and intermediate waters is the primary mechanism for moving anthropogenic  $\text{CO}_2$  to intermediate depths. The spatial distribution of anthropogenic  $\text{CO}_2$  in these intermediate waters is illustrated with the  $27.3 \sigma_\theta$  surface (Fig. 4B), whose mean depth is about 900 m. As with the  $26.0 \sigma_\theta$  surface, anthropogenic  $\text{CO}_2$  concentrations decrease away from the outcrop. On this deeper surface, however, slower ventilation results in stronger gradients and large areas where the anthropogenic  $\text{CO}_2$  is below detection level. The Atlantic contains substantially higher anthropogenic  $\text{CO}_2$  concentrations on the  $27.3 \sigma_\theta$  surface than the other basins, due in part to faster ventilation, but also because of the more favorable Revelle factor. Although the formation of intermediate, mode, and deep waters provides the primary mechanism for moving anthropogenic  $\text{CO}_2$  into the ocean interior, the magnitude and distribution of the anthropogenic signal can be quite different depending on the nature of the water mass. As examples, some of the dominant intermediate water masses are outlined in Fig. 2 (14).

Antarctic Intermediate Water (AAIW) is formed in the Southern Ocean from upwelled Circumpolar Deep Water in the vicinity of the Subantarctic Front between  $45^\circ$  and  $55^\circ\text{S}$  and is then subducted and transported northward at intermediate depths. Immediately north of the AAIW, sub-Antarctic Mode Water (SAMW) forms north of the sub-Antarctic Front and contains a greater component of subtropical water than AAIW and is also subducted into the main thermocline of the ocean interior. While at the surface, these water masses appear to take up large amounts of anthropogenic  $\text{CO}_2$  from the atmosphere as a result of both high wind speeds enhancing gas transfer and low initial anthropogenic  $\text{CO}_2$  content. These subducted intermediate and mode waters contain high concentrations of anthropogenic  $\text{CO}_2$ , which are transported equatorward and downward, as clearly evidenced by the deepening of anthropogenic  $\text{CO}_2$  penetration in Fig. 2. This transport plus the large volumetric contribution of the water masses to the Southern Hemisphere thermocline leads to high anthropogenic  $\text{CO}_2$  inventories, estimated to exceed  $20 \text{ Pg C}$  (14).

About  $3.2 \text{ Pg}$  of anthropogenic carbon is found in the North Pacific Intermediate Water (NPIW). Unlike the AAIW that typically delineates the lower limit of the anthropogenic penetration, a substantial amount of anthropogenic  $\text{CO}_2$  can be found deeper than the NPIW at the latitude of the section shown in Fig. 2B. NPIW is not the only intermediate-type water mass formed in the North Pacific, and the complex interplay of different intermediate-type waters in the North Pacific makes it difficult to attribute the anthropogenic signal to any one specific intermediate water mass in this region.

Nearly  $3 \text{ Pg C}$  can be found in the intermediate waters of the northern Indian Ocean (Fig. 2C). The Indian Ocean differs from the other oceans because of its land-locked northern boundary. Anthropogenic  $\text{CO}_2$  in the tropical north Indian Ocean generally penetrates deeper than in the tropical Atlantic and Pacific. This primarily reflects the introduction of relatively young, dense waters that

are high in anthropogenic  $\text{CO}_2$  from the Red Sea and the Persian Gulf (8, 15–16). Excess evaporation in these regions increases the salinity and density of the waters, which sink and carry the anthropogenic  $\text{CO}_2$  with them. As these waters flow into the northern Indian Ocean at intermediate depths, they mix and spread equatorward across the northern Indian Ocean.

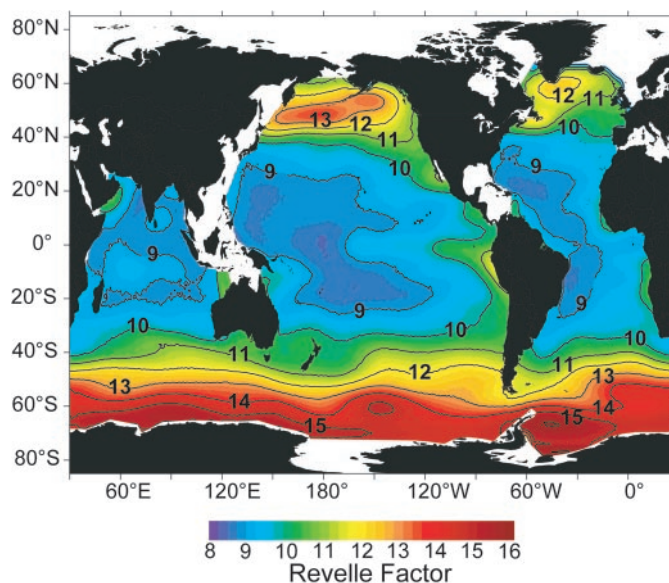


**Fig. 3.** Map of the 1994 distribution of Revelle factor,  $(\delta\text{PCO}_2/\delta\text{DIC})/(\text{PCO}_2/\text{DIC})$ , averaged for the upper 50 m of the water column. A high Revelle factor indicates that, for a given atmospheric  $\text{CO}_2$  perturbation, the oceanic equilibrium concentration of anthropogenic  $\text{CO}_2$  will be lower than that for low-Revelle factor waters. The current Revelle factors are about one unit higher than they were in the preindustrial ocean.

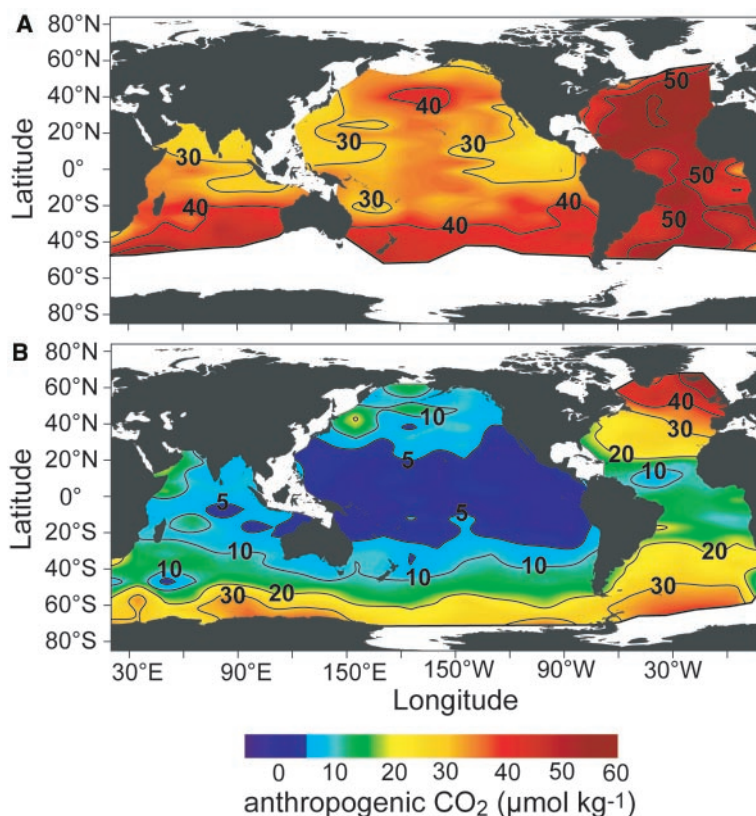


**Fig. 4.** Maps of anthropogenic  $\text{CO}_2$  on the (A)  $26.0$  and (B)  $27.3$  potential density surfaces. Bold lines at the edge of the colored region indicate areas where the density surface outcrops. The highest values are generally observed closest to the outcrop and decrease toward the equator.

Globally, only 7% of the total anthropogenic CO<sub>2</sub> is found deeper than 1500 m. The only place where large concentrations of anthropogenic CO<sub>2</sub> penetrate to mid and abyssal depths is the North Atlantic, as a result of the formation and downward spreading of Labrador Sea Water and North Atlantic Deep Water (NADW). Moving southward away from the formation region, the concentration of anthropogenic CO<sub>2</sub> in NADW decreases because the older waters were exposed to lower atmospheric CO<sub>2</sub> perturbations, and because of mixing with adjacent bottom waters containing little or no anthropogenic CO<sub>2</sub>. In total, nearly 7 Pg of anthropogenic carbon is associated with NADW (14). Thus, NADW contains substantially less anthropogenic CO<sub>2</sub> than AAIW, even though NADW has a tremendous impact on the large-scale circulation of the ocean.

There is little anthropogenic CO<sub>2</sub> associated with Antarctic Bottom Water, although exact reconstructions of the anthropogenic CO<sub>2</sub> concentration in this water mass were hampered because of limited carbon data available in regions where these bottom waters are forming. The low anthropogenic CO<sub>2</sub> inventories in these water masses are thought to result from a very high Revelle factor (Fig. 3), the limited contact with the surface before being transported into the ocean interior, and the physical barriers to CO<sub>2</sub> uptake from the presence of sea-ice (17). In addition, the anthropogenic CO<sub>2</sub> signals acquired at the surface are quickly diluted with older waters that contain no anthropogenic CO<sub>2</sub> as they sink into the abyssal ocean.

Because most of the deep ocean waters have not been in contact with the atmosphere during the anthropocene (18), the 1994 inventory of anthropogenic CO<sub>2</sub> in the ocean is only ~15% of the inventory it would have if the average surface concentration of anthropogenic CO<sub>2</sub> (56 μmol kg<sup>-1</sup>) were found throughout the ocean. This scenario, however, does not account for the Revelle factor, which makes the uptake capacity of the deep and intermediate

waters much lower than that of the surface waters. Calculating the DIC increase from an 80 parts per million (ppm) change in global ocean PCO<sub>2</sub> values (equivalent to the 1994 atmospheric CO<sub>2</sub> increase from preindustrial) implies that the 1994 inventory is ~30% of the ocean potential at that time.

**The ocean's role in the global carbon cycle.** The global ocean inventory estimated here permits us, for the first time, to place observational constraints on the anthropogenic CO<sub>2</sub> budget for the anthropocene. In particular, it permits us to estimate the magnitude of the time-integrated terrestrial carbon balance, which cannot be easily deduced from observations. We first consider the anthropogenic budget terms that are relatively well constrained. Over the anthropocene, about 244 ± 20 Pg C was emitted into the atmosphere as a result of the burning of fossil fuels and cement production (19) (Table 1). About two-thirds of these emissions have remained in the atmosphere, increasing the atmospheric CO<sub>2</sub> concentration from about 281 ± 2 ppm in 1800 (20) to 359 ± 0.4 ppm in 1994 (21), which translates to an increase of 165 Pg C. Subtracting our ocean inventory estimate of 118 ± 19 Pg C and the atmospheric inventory change from the integrated fossil-fuel emissions constrains the net carbon balance of the terrestrial biosphere to be a net source of 39 ± 28 Pg C for the period between 1800 and 1994. Therefore, the ocean has constituted the only true net sink for anthropogenic CO<sub>2</sub> over the past 200 years. Without this oceanic uptake, atmospheric CO<sub>2</sub> would be about 55 ppm higher today than what is currently observed (~380 ppm).

The terrestrial net source represents a balance between CO<sub>2</sub> emissions from land-use change, and an uptake of CO<sub>2</sub> by the terrestrial biosphere. Emissions from land-use change are ill-constrained. By comparing carbon storage between potential natural vegetation and present-day land cover, de Fries *et al.* (22) estimated a total loss of about 180 to 200 Pg C since the mid-holocene. Using a

carbon accounting model for land-use change, Houghton and Hackler (2) estimated a carbon loss of about 143 Pg C for the period from 1850 to 1994, with an uncertainty of about 50%. Extrapolating their estimate back to 1800 gives a loss of about 160 Pg C for the anthropocene. Comparisons of land-use change emissions between different estimates for the past two decades reveal, however, that Houghton and Hackler's estimates tend to be nearly twice as large as those of others (23). Taking this factor into account and the large uncertainty associated with these estimates, we adopt a range of 100 to 180 Pg C for land-use change emissions between 1800 and 1994. With this range, we infer that the terrestrial biosphere must have taken up between 61 and 141 Pg C from the atmosphere over the anthropocene.

It is interesting to contrast this anthropogenic CO<sub>2</sub> budget over the anthropocene with that over the past two decades (23). Note that the emissions from fossil fuel and cement production in the decades of the 1980s and 1990s are nearly half of the anthropocene emissions (Table 1). The airborne fraction, i.e., the fraction of the combined fossil-fuel and land-use emissions that remains in the atmosphere, is statistically indistinguishable between the two periods, i.e., 39 to 48% for the anthropocene versus ~46% for 1980 to 1999 (Table 1). There is an indication, although not statistically significant, that the ocean-uptake fraction has decreased from 28 to 34% to about 26%, whereas the sink strength of the terrestrial biosphere appears to have remained constant within the large uncertainty bounds (18 to 33% versus 28%).

**Future changes.** On the time scales of several thousands of years, it is estimated that ~90% of the anthropogenic CO<sub>2</sub> emissions will end up in the ocean (24). Because of the slow mixing time of the ocean, however, the current oceanic uptake fraction is only about one-third of this value. Studies of the coupled carbon-climate system have suggested that on decadal time scales, the ocean may become a less efficient sink for anthropogenic CO<sub>2</sub> because of positive feedbacks in the coupled carbon-climate system (25)—consistent with the suggestion of a decreasing ocean-uptake fraction noted from Table 1.

There is a potential for both positive and negative feedbacks between the ocean and atmosphere, including changes in both the physics (e.g., circulation, stratification) and biology (e.g., export production, calcification) of the ocean. These processes are still not well understood. On the time scales of decades to centuries, however, most of the known chemical feedbacks are positive. If the surface ocean PCO<sub>2</sub> concentrations continue to increase in proportion with the atmospheric CO<sub>2</sub> increase, a doubling of atmospheric

**Table 1.** Anthropogenic CO<sub>2</sub> budget for the anthropocene (1800 to 1994) and for the decades of the 1980s and 1990s.

CO <sub>2</sub> sources and sinks	1800 to 1994 (Pg C)*	1980 to 1999 (Pg C)¶
<i>Constrained sources and sinks</i>		
(1) Emissions from fossil fuel and cement production	244† ± 20	117 ± 5
(2) Storage in the atmosphere	-165‡ ± 4	-65 ± 1
(3) Uptake and storage in the ocean	-118§ ± 19	-37 ± 8
<i>Inferred net terrestrial balance</i>		
(4) Net terrestrial balance = [-(1) - (2) - (3)]	39 ± 28	-15 ± 9
<i>Terrestrial balance</i>		
(5) Emissions from land-use change	100 to 180	24 ± 12
(6) Terrestrial biosphere sink = [-(1) - (2) - (3)] - (5)	-61 to -141	-39 ± 18

\*Errors as estimated by respective sources; errors of sums and differences are calculated by quadratic error propagation. †From (19), with an error estimate of ±8%. ‡Calculated from the change in atmospheric PCO<sub>2</sub> (1800: 281 ± 2 ppm; 1994: 359 ± 0.4 ppm). §This study includes anthropogenic CO<sub>2</sub> storage in marginal seas and the Arctic Ocean. ||Based on (2); see text for details. ¶From (23), integrated for the period 1980 to 1999.



CO<sub>2</sub> from preindustrial levels will result in a 30% decrease in carbonate ion concentration and a 60% increase in hydrogen ion concentration. As the carbonate ion concentration decreases, the Revelle factor increases and the ocean's ability to absorb more CO<sub>2</sub> from the atmosphere is diminished. The impact of this acidification can already be observed today and could have ramifications for the biological feedbacks in the future (26). If indeed the net feedbacks are primarily positive, the required socioeconomic strategies to stabilize CO<sub>2</sub> in the future will be much more stringent than in the absence of such feedbacks. Future studies of the carbon system in the oceans should be designed to identify and quantitatively assess these feedback mechanisms to provide input to models that will determine the ocean's future role as a sink for anthropogenic CO<sub>2</sub>.

## References and Notes

1. P. J. Crutzen, E. F. Stoermer, *Global Change Newsletter*, **41**, 12 (2000).
2. R. A. Houghton, J. L. Hackler, in *Trends: A Compendium of Data on Global Change* (Carbon Dioxide Information Analysis Center, Oak Ridge National Laboratory, TN, 2002), <http://cdiac.esd.ornl.gov/trends/landuse/houghton/houghton.html>.
3. C. Prentice et al., in *Climate Change 2001: The Scientific Basis. Contribution of Working Group I to the Third Assessment Report of the Intergovernmental Panel on Climate Change*, J. T. Houghton et al., Eds. (Cambridge Univ. Press, New York, 2001), pp. 183–237.
4. D. W. R. Wallace, in *Ocean Circulation and Climate*, G. Siedler, J. Church, W. J. Gould, Eds. (Academic Press, San Diego, CA, 2001), pp. 489–521.
5. R. M. Key et al., in preparation.
6. Bottle data and 1° gridded distributions are available through the GLODAP Web site ([http://cdiac.esd.ornl.gov/oceans/glodap/Glodap\\_home.htm](http://cdiac.esd.ornl.gov/oceans/glodap/Glodap_home.htm)).
7. N. Gruber, J. L. Sarmiento, T. F. Stocker, *Global Biogeochem. Cycles* **10**, 809 (1996).
8. C. L. Sabine et al., *Global Biogeochem. Cycles* **13**, 179 (1999).
9. C. L. Sabine et al., *Global Biogeochem. Cycles* **16**, 1083, 10.1029/2001GB001639 (2002).
10. K. Lee et al., *Global Biogeochem. Cycles* **17**, 1116, 10.1029/2003GB002067 (2003).
11. Materials and methods are available as supporting material on Science Online.
12. R. Revelle, H. E. Suess *Tellus* **9**, 18 (1957).
13. T. Takahashi, J. Olafsson, J. G. Goddard, D. W. Chipman, S. C. Sutherland, *Global Biogeochem. Cycles* **7**, 843 (1993).
14. Five intermediate water masses and NADW were defined using the following temperature (*T*) and salinity (*S*) properties: Pacific AAIW: 33.8 < *S* < 34.5 and 2 < *T* < 10; NPIW: 5 < 34.3 and 5 < *T* < 12; Indian AAIW: 33.8 < *S* < 34.5 and 2 < *T* < 10; Red Sea Water: 5 > 34.8 and 5 < *T* < 14; Atlantic AAIW: 33.8 < *S* < 34.8 and 2 < *T* < 6; NADW: 34.8 < *S* < 35 and 1.5 < *T* < 4. Water mass inventories were determined by summing up the gridded anthropogenic CO<sub>2</sub> values within a region defined by the *T* and *S* limits using the Levitus World Ocean Atlas 2001 salinity and temperature fields.
15. A. Papaud, A. Poisson, *J. Mar. Res.* **44**, 385 (1986).
16. S. Mecking, M. Warner, *J. Geophys. Res.* **104**, 11087 (1999).
17. A. Poisson, C.-T. A. Chen, *Deep-Sea Res. Part A* **34**, 1255 (1987).
18. M. Stuiver, P. D. Quay, H. G. Ostlund, *Science* **219**, 849 (1983).
19. G. Marland, T. A. Boden, R. J. Andres, in *Trends: A Compendium of Data on Global Change* (Carbon Dioxide Information Analysis Center, Oak Ridge National Laboratory, TN, 2003), [http://cdiac.esd.ornl.gov/trends/emis/meth\\_reg.htm](http://cdiac.esd.ornl.gov/trends/emis/meth_reg.htm).
20. D. M. Etheridge et al., *J. Geophys. Res.* **101**, 4115 (1996).
21. C. D. Keeling, T. P. Whorf, in *Trends: A Compendium of Data on Global Change* (Carbon Dioxide Information Analysis Center, Oak Ridge National Laboratory, TN, 2004), <http://cdiac.esd.ornl.gov/trends/co2/sio-keel.htm>.
22. R. S. de Fries, C. B. Field, I. Fung, G. J. Collatz, L. Bounoua, *Global Biogeochem. Cycles* **13**, 803 (1999).
23. C. L. Sabine et al., in *The Global Carbon Cycle: Integrating Humans, Climate, and the Natural World*, SCOPE 62, C. B. Field, M. R. Raupach, Eds. (Island Press, Washington, DC, 2004), pp. 17–44.
24. D. E. Archer, H. Kheshgi, E. Maier-Reimer, *Global Biogeochem. Cycles* **12**, 259 (1998).
25. N. Gruber et al., in *The Global Carbon Cycle: Integrating Humans, Climate, and the Natural World*, SCOPE 62, C. B. Field, M. R. Raupach, Eds. (Island Press, Washington, DC, 2004), pp. 45–76.
26. R. A. Feely et al., *Science* **305**, 362 (2004).
27. We thank all individuals who contributed to the global data set compiled for this project, including those responsible for the hydrographic, nutrient, oxygen, carbon, and chlorofluorocarbon measurements, and the chief scientists. The amount of work that went into collecting, finalizing, and synthesizing these data in a manner that makes a publication like this possible can never be properly acknowledged. This work was funded by grants from NOAA/U.S. Department of Energy and NSF. Partial support for K.L. was also provided by the Advanced Environmental Biotechnology Research Center at Pohang University of Science and Technology. This is Pacific Marine Environmental Laboratory contribution number 2683.

## Supporting Online Material

[www.sciencemag.org/cgi/content/full/305/5682/367/DC1](http://www.sciencemag.org/cgi/content/full/305/5682/367/DC1)  
Materials and Methods  
Fig. S1  
Table S1

2 March 2004; accepted 8 June 2004

# Mapping the Antigenic and Genetic Evolution of Influenza Virus

Derek J. Smith,<sup>1,2\*</sup> Alan S. Lapedes,<sup>3\*</sup> Jan C. de Jong,<sup>2</sup>  
Theo M. Bestebroer,<sup>2</sup> Guus F. Rimmelzwaan,<sup>2</sup>  
Albert D. M. E. Osterhaus,<sup>2</sup> Ron A. M. Fouchier<sup>2\*</sup>

The antigenic evolution of influenza A (H3N2) virus was quantified and visualized from its introduction into humans in 1968 to 2003. Although there was remarkable correspondence between antigenic and genetic evolution, significant differences were observed: Antigenic evolution was more punctuated than genetic evolution, and genetic change sometimes had a disproportionately large antigenic effect. The method readily allows monitoring of antigenic differences among vaccine and circulating strains and thus estimation of the effects of vaccination. Further, this approach offers a route to predicting the relative success of emerging strains, which could be achieved by quantifying the combined effects of population level immune escape and viral fitness on strain evolution.

Much of the burden of infectious disease today is caused by antigenically variable pathogens that can escape from immunity induced by prior infection or vaccination. The degree to which immunity induced by one strain is effective against another is mostly dependent on the antigenic difference between the strains; thus, the analysis of antigenic differences is critical for surveillance and vaccine strain selection. These differences are measured in the laboratory in various binding assays (1–3). Such assays give an approximation of antigenic differences, but are generally considered unsuitable for quantitative analyses. We present a method, based

on the fundamental ideas described by Lapedes and Farber (4), that enables a reliable quantitative interpretation of binding assay data, increases the resolution at which antigenic differences can be determined, and facilitates visualization and interpretation of antigenic data. We used this method to study quantitatively the antigenic evolution of influenza A (H3N2) virus, revealing both similarities to, and important differences from, its genetic evolution.

Influenza viruses are classic examples of antigenically variable pathogens and have a seemingly endless capacity to evade the immune response. Influenza epidemics in humans cause an estimated 500,000 deaths worldwide per year (5). Antibodies against the viral surface glycoprotein hemagglutinin (HA) provide protective immunity to influenza virus infection, and this protein is therefore the primary component of influenza vaccines. However, the antigenic structure of HA has changed significantly over time, a process known as antigenic drift (6), and in most years, the influenza vaccine has to be up-

<sup>1</sup>Department of Zoology, University of Cambridge, Downing Street, Cambridge CB2 3EJ, UK. <sup>2</sup>National Influenza Center and Department of Virology, Erasmus Medical Center, Dr. Molewaterplein 50, 3015GE Rotterdam, Netherlands. <sup>3</sup>Theoretical Division, T-13, MS B213, Los Alamos National Laboratory, Los Alamos, NM 87545, USA.

\*These authors contributed equally to this work.

†To whom correspondence should be addressed. E-mail: dsmith@zoo.cam.ac.uk